Missing data in aftershock sequences: Explaining the deviations from scaling laws

Sabine Lennartz* and Armin Bunde
Institut für Theoretische Physik III, Justus-Liebig-Universität Giessen, 35392 Giessen, Germany

Donald L. Turcotte
Department of Geology, University of California, Davis, California 95616, USA
(Received 29 April 2008; revised manuscript received 11 July 2008; published 14 October 2008)

In this paper we extend the branching aftershock sequence model to study the role of missing data at short times and small amplitudes after a mainshock. We apply this model, which contains three parameters characterizing the missing data, to the magnitude and temporal statistics of four aftershock sequences in California. We find that the observed time-dependent deviations of the frequency-magnitude scaling from the Gutenberg-Richter power law dependency can be described quantitatively by the model. We also show that, for the same set of parameters, the model is able to explain quantitatively the observed magnitude-dependent deviations of the temporal decay of aftershocks from Omori's law. In addition, we show that the same sets of data can also reproduce quite well the various functional forms of the probability density functions of the return times between consecutive events with magnitudes above a prescribed threshold, as well as the violation of scaling at short and intermediate time scales.

DOI: 10.1103/PhysRevE.78.041115 PACS number(s): 02.50.Ey, 91.30.Ab, 89.75.Da

I. INTRODUCTION

All earthquakes have associated aftershock sequences. Apart from Båth's law for the difference in magnitudes between the mainshock and the largest aftershock [1], aftershock sequences are generally characterized by two scaling laws: (1) Gutenberg-Richter (GR) frequency-magnitude scaling [2] and (2) Omori's law for the temporal decay of aftershocks [3]. But there exist systematic deviations from both scaling laws at low magnitudes and small time windows after the mainshock. An essential question is whether these differences are real (and generated, for example, by correlations) or are due to aftershock catalogs that are not complete at early times after a mainshock. It is well known that, at early times after a mainshock, due to the large amount of seismic noise, not all (small) aftershocks can be detected. It has been suggested by Helmstetter *et al.* [4] that there exists a time-dependent threshold $m_c(M,t)=M-4.5-0.75\log_{10}(t)$ with $m_c \geqslant 2$ where M is the mainshock magnitude and t is the time (in days) elapsed after this mainshock, above which the catalog is complete. For further discussions of this problem, see [5–9].

Here we consider four Californian aftershock sequences in a time window of 365 days after the mainshock: Landers ($M=7.3$, June 28, 1992), Hector Mine ($M=7.1$, October 16, 1999), Northridge ($M=6.7$, January 17, 1994), and Parkfield ($M=6.0$, September 28, 2004) [10]. We model them by a a self-similar, epidemic-type branching model for aftershock sequences [11–13] (where we fit the parameters to the real sequences). Then we use probabilistic arguments in conjunction with the time-dependent threshold $m_c(M,t)$ to model the amount of missing data. We show that by this extension, which involves three fitting parameters, the observed time-dependent deviations of the frequency-magnitude scaling from the GR scaling can be explained quantitatively. After having evaluated the fitting parameters by the frequency-magnitude scaling, we use the same data sets to explain (without any additional fitting parameters) the observed anomalies in the magnitude dependency of the temporal decay of aftershocks.

As a further study of the role of the missing data, we also analyze the series of return times between consecutive events with magnitudes above a prescribed threshold. We find that the functional form of the probability density functions (PDFs) of the return times, which is often an important tool in risk estimation (see, e.g., [14,15] and references therein), is not universal, but differs for the different aftershock sequences and violates scaling at small and intermediate time scales. We show that our model can also reproduce these anomalies without any additional parameter.

II. BRANCHING MODEL

For simulations of earthquakes and their aftershock sequences, several branching models have been evaluated. Among them are the epidemic-type aftershock sequence (ETAS) model [16–18] and the related branching aftershock sequence (BASS) model [11,12,19]; see also Felzer *et al.* [13]. The concept of both models is the following. Each parent earthquake creates its own aftershock sequence of daughter earthquakes, and each daughter earthquake then becomes a parent which generates second-order aftershocks. This process is then carried out to higher orders. Both models utilize GR scaling [2] and Omori's law [3]. One difference between the ETAS and BASS models is that the ETAS model prescribes a branching ratio in order to constrain the number of aftershocks of each generation, while in the BASS model a modified form of Båth's law [20] is used. The other difference between the models is, that the number of aftershocks of a parent event with magnitude m_p is proportional to $10^{\alpha m_p}$ with $\alpha < b$ for the ETAS model, where b is the GR scaling

*sabine.lennartz@uni-giessen.de

parameter, but $\alpha=b$ for the BASS model. Since each parent event with magnitude m_p occurs with a probability proportional to 10^{-bm_p} (GR), they trigger events proportional to $10^{-(b-\alpha)m_p}$. This means that in the ETAS model it is assumed that small earthquakes collectively dominate earthquake triggering, because their greater frequency overcomes their small individual triggering potential [21]. In the BASS model small earthquakes are as important to earthquake triggering as larger ones. For that reason the BASS model is fully self-similar, which is not the case for the ETAS model. The following simulations will be based on the BASS model.

A. Generation of the aftershock sequences

We consider a (total) aftershock sequence, which consist of several sequences of daughter earthquakes. The total sequence is governed by the GR scaling, Omori's law, and Båth's law.

The GR relation [2] for the cumulative number of aftershocks greater than a minimum magnitude $m_{\min}$ states

$$\log_{10}[N(\geqslant m_{\min})] = a - bm_{\min}. \tag{1}$$

We assume that this relation is also valid for each sequence of daughter earthquakes,

$$\log_{10}[N_{d,i}(\geqslant m_{\min})] = a_{d,i} - bm_{\min}, \tag{2}$$

where $N_{d,i}(\geqslant m_{\min})$ is the cumulative number of daughter earthquakes of a parent event i with magnitude $m_{p,i}$. This assumption is consistent with Eq. (1) with $N(\geqslant m_{\min})=\Sigma_i N_{d,i}(\geqslant m_{\min})$ and

$$10^a = \sum_i 10^{a_{d,i}}. \tag{3}$$

Båth's law [20] states that the magnitude of the largest aftershock inferred from the GR relation (1) is required to be a fixed value $\Delta m^* \approx 1.2$ less than the magnitude of the mainshock M, that is,

$$N[\geqslant (M - \Delta m^*)] = 1. \tag{4}$$

It must be emphasized that Δm^* is not the magnitude difference between the mainshock and the largest aftershock $\Delta m = M - m_{as,\max}$. Substituting (4) into (1) requires

$$a = b(M - \Delta m^*). \tag{5}$$

We also assume that the modified form of Båth's law is valid for each sequence of daughter earthquakes with a parent earthquake with magnitude $m_{p,i}$,

$$a_{d,i} = b(m_{p,i} - \Delta m^*_{d,i}), \tag{6}$$

where $\Delta m^*_{d,i}$ is the difference between the parent magnitude and the largest daughter earthquake inferred from the GR relation. We also assume that $\Delta m^*_{d,i}$ does not depend on the parent magnitude, and skip the index i in the following. Substitution of (5) and (6) into (3) gives

$$10^{-b\Delta m^*} = 10^{-b\Delta m^*_d} + \sum_{i\neq 0} 10^{b(m_{p,i}-M-\Delta m^*_d)}. \tag{7}$$

Since the sum in Eq. (7) is positive, the value for Δm^*_d has to be a little larger than $\Delta m^* \approx 1.2$. For the sake of generality, we do not consider the actual Båth parameter for each sequence as a constant, but choose it randomly from a Gaussian distribution with mean 1.4 and standard deviation 0.4. For larger standard deviations, the system becomes unstable. We found that the possible choices for the mean of Δm^*_d are between 1.3 and 1.5. For smaller mean values too many events will be generated and for larger mean values too few compared to the original data.

TABLE I. Parameters of the branching model and optimized parameters for the missing data for the four aftershock sequences Landers, Hector Mine, Northridge, and Parkfield. The values for p, M, c, and b are also listed in [23,24]. The error bars for γ_1, m_2, and γ_2 are 0.2.

Earthquake	p	M	c (days)	b	γ_1	m_2	γ_2
Landers	1.22	7.3	0.08	0.98	2.0	1.5	1.5
Hector Mine	1.21	7.1	0.024	1.01	1.8	1.4	1.5
Northridge	1.18	6.7	0.012	0.91	1.2	1.4	1.5
Parkfield	1.09	6.0	0.00395	0.89	0.7	1.2	1.5

Finally, the generalized form of Omori's law [22] states

$$r(t) = \frac{dN}{dt} = \frac{1}{\tau(1 + t/c)^p}. \tag{8}$$

The characteristic time c is a measure of the time delay before the onset of aftershock activity. Certainly c must be finite in order to prevent a small time singularity. In this paper we consider c as a constant. As for the GR scaling and for Båth's law, we assume that this law is also valid for each sequence of daughter earthquakes:

$$r_{d,i}(t) = \frac{dN_{d,i}}{dt} = \frac{\Theta(t - t_i)}{\tau_{d,i}[1 + (t - t_i)/c]^p}. \tag{9}$$

t_i is here the time of occurrence of the parent event and Θ is the Heaviside function. If one sums now over all sequences of daughter earthquakes, the rate is still approximately constant for $t<c$ and a decaying power law for very large times. So this assumption is also justified.

To generate a complete aftershock sequence consisting of several generations of aftershocks, we start with the first generation. The mainshock M is predefined, for example $M=7.3$ for modeling the Landers aftershock sequence. This mainshock is the parent event of the first generation with magnitude m_p.

The cumulative number of all daughter earthquakes N_d with magnitudes greater than $m_{\min}$ is then given by (2) and (6):

$$N_d = 10^{b(m_p - \Delta m^*_d - m_{\min})}. \tag{10}$$

The b value can be fitted straightforwardly from the real data when large time windows (of the order of one year) are considered. The fitted values from Landers, Hector Mine Northridge, and Parkfield are listed in Table I. To obtain an integer value for the actual value N_d we use the standard rounding procedure.

The magnitude of each of the N_d daughter earthquakes is picked randomly from the GR probability distribution function p,

$$p(m) = b \ln(10) \times 10^{-b(m-m_{\min})}. \tag{11}$$

The next step is specify the time of occurrence of each daughter earthquake. The rate of occurrence of daughter earthquakes r at a time t after the parent earthquake, which happened at time $t_0=0$, is given by (9), where the parameters c and p are constrained by observations of the original aftershock record for large magnitudes, where the data set can be considered as complete. The fitted values we use are listed in Table I. The total number of daughter earthquakes from (9) is

$$N_d = \int_0^\infty r_d(t)dt = \frac{c}{\tau_d(p-1)}. \tag{12}$$

From (9) and (12) the probability distribution function p of the times of occurrence t of daughter earthquakes is given by

$$p(t) = \frac{p-1}{c(1+t/c)^p}. \tag{13}$$

The time of occurrence of each of the daughter earthquakes is picked randomly from this distribution, which is independent of the chosen magnitude. Alternatively, we could first choose the occurrence times by Eq. (13) and then choose the magnitudes randomly by Eq. (11). Thus the magnitudes remain uncorrelated in the version of the BASS model we use here. Since we can compare our results only with real aftershock sequences up to one year after a large mainshock, we do not consider all later events.

This completes the first generation of aftershocks. Next we assume that each aftershock of the first generation can create its own aftershock sequence in the second generation. The procedure is the same as above. The second generation then can create, in exactly the same manner, the third generation of aftershocks and so on.

B. Missing data

Figure 1 shows the magnitudes of the four Californian aftershock sequences Landers, Hector Mine, Northridge, and Parkfield plotted as a function of the time (in days) elapsed after the mainshock. One can clearly see that there are no small events in the very beginning. The reason for this may be correlations, where large events are preferentially followed by large events; see, for example, [25,26]. Another reason for this may be that at early times the catalogs are not complete for small events because they are lost in the seismic noise generated by large early events, where according to Fig. 1 the completeness depends somehow on the mainshock magnitude M and the time t (in days) elapsed after the mainshock. Here we follow this direction. It has been suggested by Helmstetter *et al.* [4] that the catalogs are complete only above a threshold

$$m_c(M,t) = \max[m_1(M,t), m_2] \tag{14}$$

with

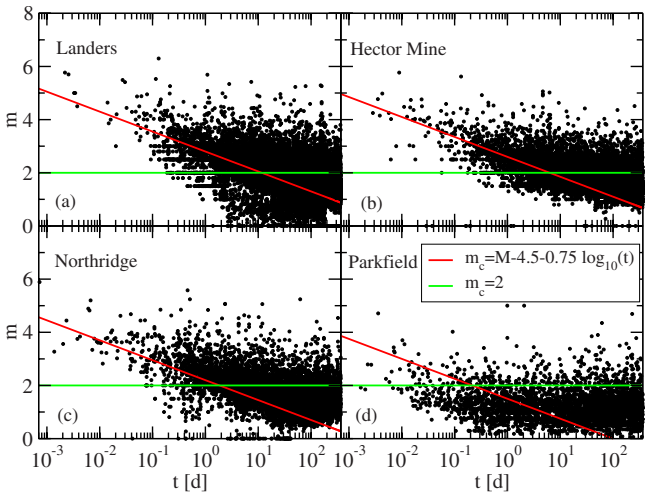

FIG. 1. (Color online) Magnitudes m of the four Californian aftershock sequences (a) Landers, (b) Hector Mine, (c) Northridge, and (d) Parkfield detected at time t (in days) after the mainshock. One can clearly see that the catalogs are not complete at short times after the mainshock because of small missing data points. The straight lines are the thresholds proposed by Helmstetter *et al.* [4] [see also Eqs. (15) and (16)] above which the catalogs should be complete.

$$m_1(M,t) = M - 4.5 - 0.75 \log_{10}(t) \tag{15}$$

and

$$m_2 = 2. \tag{16}$$

The motivation for the first threshold m_1 is that after a mainshock it takes some time until the earth has calmed down, such that new events can be observed again. The second threshold m_2 is motivated by the (time-independent) sensibility of the seismographs. Events below m_2 are so weak that the seismographs do not always recognize them as separate events.

Since mainshocks and aftershocks cannot be distinguished *a priori*, we assume that relations (14)–(16) do not hold exclusively for a mainshock but for any shock with magnitude M and t the time elapsed after this event. But the condition does not tell us which data are missing. Clearly, as seen in Fig. 1, not all data below the threshold from Eq. (14) can be considered as missing. Only a certain fraction of magnitudes below $m_c(M,t)$ can be observed, and the probability that a given event below the threshold occurs should depend on its magnitude. Here we assume that magnitudes m below m_1 (m_2) from Eq. (14) occur with a probability

$$p_1(m_1,m) = 10^{-\gamma_1(m_1-m)} \tag{17}$$

and

$$p_2(m_2,m) = 10^{-\gamma_2(m_2-m)}. \tag{18}$$

This assumption is motivated by the Boltzmann distribution $e^{-\beta V}$, where $m_c - m$ plays the role of the potential V and γ the role of the inverse temperature β. Here we consider γ_1, γ_2, and m_2 as fitting parameters. In the limit $\gamma_1=\gamma_2=0$ all events

are observed, while in the opposite limit $\gamma_1=\gamma_2=\infty$ all data below m_1 and m_2 are deleted.

Accordingly, for modeling an incomplete aftershock sequence we proceed as follows. After having obtained a complete aftershock sequence (described in Sec. II A), we check for each aftershock if it is above or below $m_c(m_1,m_2)$. If it is above, this event is observed. If it is below, we choose two random numbers r_1 and r_2 between 0 and 1. Only if r_1 is below p_1 and r_2 is below p_2 will this event be observed. Otherwise it is deleted from the catalog.

We would like to emphasize that γ_1, γ_2, and m_2 are the only fitting parameters for describing the missing data, since the threshold $m_c(M,t)$ from Eq. (15) does not include any fitting parameter. Of course, γ_1, γ_2, and m_2 depend on the functional form of m_1 and for a different choice of m_1 we will obtain different values for these parameters. In this paper, in order to minimize the number of fitting parameters, we have chosen m_1 from the suggestion of Helmstetter *et al.* [4]. In the following, we will show that by an optimum fit of γ_1, γ_2, and m_2 we can quantitatively describe the time-dependent deviations of the frequency-magnitude scaling from GR scaling. Then we will take these fitting parameters for granted and show that we obtain a parameter-free description of the magnitude dependence of the deviations from Omori's law, as well as a parameter-free description of the PDF of the return times between consecutive events above some magnitude threshold for all the aftershock sequences we consider.

III. RESULTS

Next we consider the four Californian aftershock sequences Landers, Hector Mine, Northridge, and Parkfield and compare them with modeled sequences with $m_{\min}=0$ for the two (unrealistic) limiting cases $\gamma_1=\gamma_2=0$ and $\gamma_1=\gamma_2=\infty$ with $m_2=2$, which we will refer to as model 1 and model 2, respectively, as well as for the best fit to the real data, which we call model 3. In the modeled sequences, the parameter p, M, c, and b are taken from the real data (see Table I) and Δm_d^* is chosen randomly from a Gaussian distribution with mean 1.4 and variance 0.2. This choice guarantees that the total number of shocks after one year (see, e.g., the upper curves in the left column of Fig. 2) is the same as for the real data.

First we consider the frequency-magnitude scaling for the real and the three modeled Landers aftershock sequences in five different time windows ($t\leqslant 0.1$, 1, 10, 92, and 365 days) after the mainshock, as shown in the left-hand side of Fig. 2. Figure 2(a) shows the data of model 1 where $\gamma_1=\gamma_2=0$. The unaltered GR frequency-magnitude scaling is clearly observable, because there are no missing data. Since the parameter b is fitted from the real data, the slope in Fig. 2(a) is identical with the slope in Fig. 2(g) above the crossover magnitude.

Figure 2(c) shows the cumulative distribution of model 2 in the opposite limit where $\gamma_1=\gamma_2=\infty$ with $m_2=2$. All events below the thresholds m_1 and m_2 [Eqs. (15) and (16)] have been deleted. In this case one can see already the characteristic time-dependent crossover $m_*(t)$, which is observable in the real data [Fig. 2(g)]. Below $m_*(t)$, the cumulative number

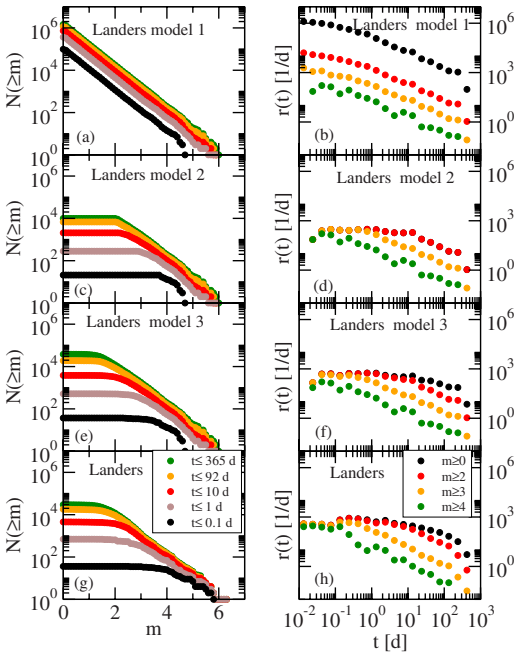

FIG. 2. (Color online) Comparison of the Landers aftershock sequence [(g) and (h)] with three model sequences [(a)–(f)]. Left column: Cumulative numbers of aftershocks with magnitudes greater than m, $N(\geqslant m)$, are given as a function of m for five different time windows ($t\leqslant 365$, 92, 10, 1, and 0.1 days from top to bottom) after the mainshock. Right column: Daily rates $r(t)$ of aftershocks with magnitudes $m\geqslant 0$, 2, 3, and 4 from top to bottom. (a) and (b) refer to the complete model (model 1), (c) and (d) to the model where all data below the thresholds proposed by Helmstetter *et al.* [4] [see also Eqs. (15) and (16)] have been removed (model 2), and (e) and (f) refer to the optimized model (model 3), where the parameters are listed in Table I. For the cumulative number of aftershocks, as well as for the daily rates, the agreement between the optimized model data (model 3) and the real data is striking.

N is constant, while above $m_*(t)$, N decays by the GR frequency-magnitude scaling. The time dependence of the crossover magnitude reflects the time dependence of the threshold m_1. If m_1 did not depend on time but was a constant depending on the magnitude of the mainshock, then the crossover would be time independent. The fact that this is not the case is, in our opinion, a clear indication of the necessity of a time-dependent threshold m_1.

But the agreement between model 2 and the real data is not perfect. Since we omitted all data below m_1 and $m_2=2$, the plateau values are too small and the crossover between plateau and GR scaling behavior is too abrupt. This points to the necessity of choosing the second threshold m_2 smaller and also of choosing finite values for γ_1 and γ_2, because then events with small magnitudes will have a finite probability to be observed. While γ_1 mainly determines the height of the plateau for small time windows, the height of the plateau for long time windows is mainly determined by the threshold m_2 and by γ_2. Accordingly, γ_1 can be used to fit the plateaus for short times, the threshold m_2 can be used to fit the crossover point for long times, and the exponent γ_2 can be used to fit the smoothness of the crossover. We find that for Landers the optimized values are $\gamma_1=2.0$, $\gamma_2=1.5$ and $m_2=1.5$. Figures

2(e) and 2(g) show that for these values the agreement between the model data and the real data is nearly perfect.

After these parameters have been specified by the GR scaling, we do not have any free parameter left for fitting to Omori's law (for different magnitudes) and the PDF of the return times. We will show in the following that the best-fitted model for the GR scaling is also the best model for Omori's law and the PDF of the return times.

The daily rates $r_m(t)$ of the four Landers aftershock sequences above magnitudes $m=0$, 2, 3, and 4 are shown in the right-hand side of Fig. 2. Again, the real Landers sequence [Fig. 2(h)] is compared with [Fig. 2(b)] model 1, [Fig. 2(d)] model 2, and [Fig. 2(f)] model 3. As expected, in Fig. 2(b) the data simply follow Omori's law with a magnitude-dependent initial rate $1/\tau$ and a constant c value. Figure 2(d) shows that model 2 already describes the data quite well. Now the time dependence of the thresholds is reflected in $r_m(t)$. For a constant threshold m_1 the daily rates $r_m(t)$ would keep satisfying Omori's law for $m > m_1$, while they would coincide for $m < m_1$. As can be seen immediately from inspecting Fig. 2(h), this is not the case for the real data. For the time-dependent threshold $m_1(t)$ the situation is different. In the time frame considered in Fig. 2, the maximum threshold occurs at $t=10^{-2}$ days and is given by $m_1(t=10^{-2}\ \text{days}) = M-3$. Accordingly, for $m > M-3$, the rate $r_m(t)$ is not affected by the missing data in the considered time frame and satisfies Omori's law. For $m < M-3$, there exists a crossover time $t_*(m)$ above which the rate also satisfies Omori's law. It can be easily shown that $t_*(m)$ is given by

$$t_*(m) = 10^{(M-4.5)/0.75 - m/0.75}. \tag{19}$$

For $t < t_*(m)$, only events above $m_1(t)$ appear and hence

$$r_m(t < t_*(m)) = r_{m_1(t)}(t). \tag{20}$$

Accordingly, for all $m < m_1(t)$, the rates collapse and are given by

$$r_{m_1(t)}(t) = \frac{p-1}{c}\frac{10^{-bm_1(t)}}{(1+t/c)^p} \tag{21}$$

$$\propto \frac{t^{0.75b}}{(1+t/c)^p}. \tag{22}$$

As a consequence, below the crossover time $t_*(m)$ the resulting Omori rate $r_m(t)$ is no longer a monotonic function of time: For $t \ll c$ it increases as $t^{0.75b}$ while for $t \gg c$ it decreases as $t^{0.75b-p}$. This nonmonotonic behavior can be observed in Figs. 2(d), 2(f), and 2(h). This figure shows that model 2 describes the real data quite well, but in the optimized version [with the same parameter values $\gamma_1=2.0$, $\gamma_2=1.5$, and $m_2=1.5$ as in Fig. 2(e)], which is shown in Fig. 2(f), we observe the best agreement between the real and the model data.

Figures 3–5 show the cumulative numbers $N(\geq m)$ and the rates $r(t)$ for the Hector Mine, Northridge, and Parkfield records. As in Fig. 2 the optimum parameters (model 3) have been obtained from a fit to the cumulative number of aftershocks in several time windows. In this sense the fits shown

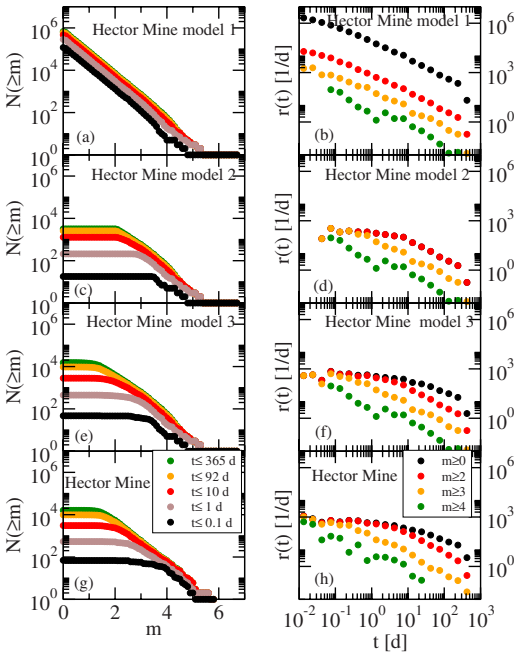

FIG. 3. (Color online) Same as Fig. 2, but for the Hector Mine aftershock sequence.

in Figs. 3(f), 4(f), and 5(f) are parameter-free. Again the agreement between the real and model data is striking. Table I lists the optimized parameters γ_1, γ_2, and m_2 for the four aftershock sequences considered. Note that γ_2 and m_2 are nearly constant, while γ_1 seems to decrease approximately linearly with decreasing mainshock magnitude M, $\gamma_1 \approx M - 5.3$.

Since the threshold m_1 also depends linearly on the mainshock magnitude M, the fraction of observed data with small

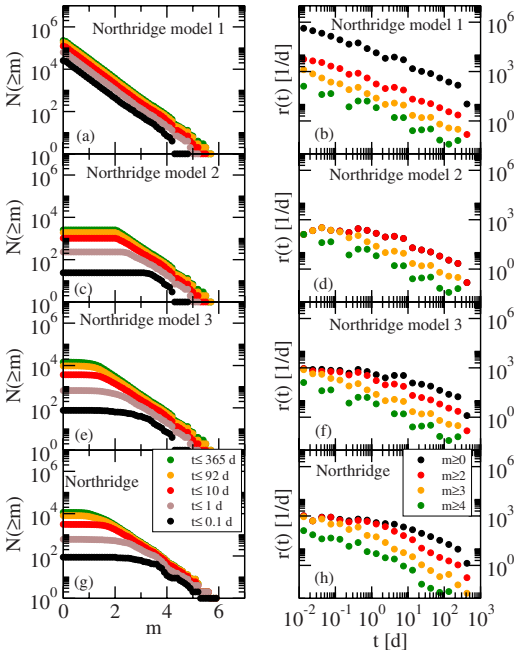

FIG. 4. (Color online) Same as Fig. 2, but for the Northridge aftershock sequence.

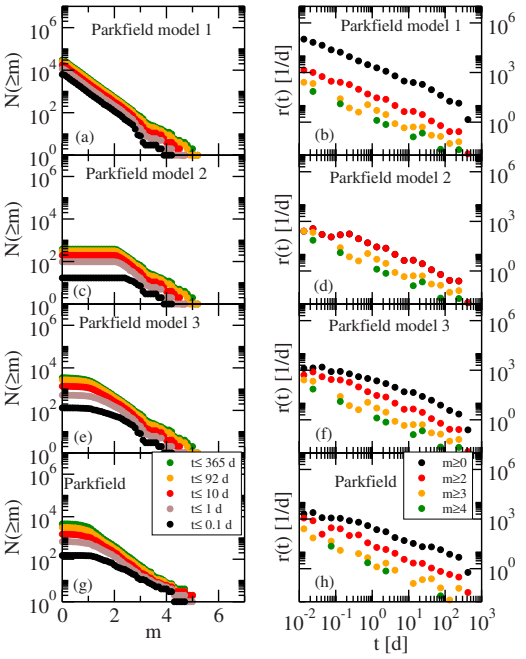

FIG. 5. (Color online) Same as Fig. 2, but for the Parkfield aftershock sequence.

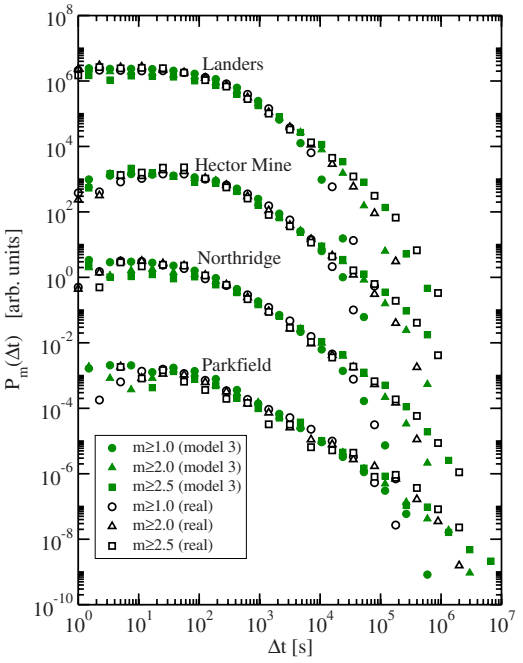

FIG. 6. (Color online) Probability density function (PDF) $P_m(\Delta t)$ of the return times Δt of four Californian aftershock sequences above the magnitude thresholds $m=1.0$ (circles), 2.0 (triangles), and 2.5 (squares). The filled symbols are the data of the optimized model, where missing data have been taken away with some probability (model 3) [see also Eqs. (17) and (18)]. The parameters are listed in Table I. The open symbols are the real data. For the sake of clarity the data of the different aftershock sequences have been shifted by a factor of 1000. For all four aftershock sequences, the agreement between the optimized model data (model 3) and the real data is nearly perfect.

magnitudes roughly decreases as $10^{-(M-5.3)^2}$. As a consequence, the incompleteness of a catalog is drastically enhanced for large mainshocks, and the time dependence of the threshold leads to the time dependence of the crossover in the GR distribution. For Landers ($M-5.3=2.0$), in Figs. 2(e) and 2(g), this time dependence is clearly observable. In contrast, after small mainshocks, the constant threshold m_2 becomes relevant. This is the case for Parkfield [$M-5.3=0.7$ in Figs. 5(e) and 5(g)], where the crossover is nearly time independent.

Next we consider the PDF, $P_m(\Delta t)$m, of the return times Δt between events with magnitudes greater than m. $P_m(\Delta t)$ is a central quantity in risk estimation and has been studied for a large number of complex systems (for references, see [14,15]). Based on studies of Californian seismicity, Bak *et al.* [27] proposed a general scaling law for return times, and a number of authors [25,28–39] have extended this work recently. In this paper, we study the PDFs of the return times between events with magnitudes $m \geqslant 1$, 2, and 2.5 for our four Californian aftershock sequences (open symbols in Figs. 6 and 7). We focus on the question of whether the optimized model (full symbols in Figs. 6 and 7) is able to describe quantitatively the different features of the PDFs of the four aftershock sequences. For the sake of clarity the PDFs of the different aftershock sequences have been shifted by a factor of 1000.

Figure 6 shows the PDFs of the return times of the observed and optimized model data. It is remarkable that both data sets collapse and cannot be distinguished *a priori* from each other. For return times above 10^4 s the PDFs become strongly magnitude dependent and decay more slowly for larger thresholds, while for return times below 10 s the data scatter. This scatter increases with decreasing magnitude of the mainshock and is thus most pronounced for the Parkfield record ($M=6.0$). The functional form of the PDF at intermediate time scales ranges from a power law behavior for Parkfield to a more curved exponential kind of behavior for Landers.

Figure 7 shows the data in a rescaled form, where the x axis is divided by the mean return time $\langle \Delta t \rangle$ and the y axis is multiplied by $\langle \Delta t \rangle$. For comparison, the figure shows also the PDF obtained from model 1 (dotted symbols). Since the model is fully self-similar, the data scale and the PDF exhibits a power law behavior at intermediate time scales, which is most pronounced for smaller values of the mainshock magnitude M.

In contrast to model 1, both observational and optimized model data spread considerably below a crossover time Δt_* which increases with increasing magnitude of the mainshock. Above Δt_* the Parkfield data show power law scaling (as for model 1) while for the other three sequences the data for different thresholds do not scale. Below Δt_* the PDFs for $m \geqslant 1$ are well below the PDFs for $m \geqslant 2.5$, while for intermediate return times they are above them.

It can be seen that this behavior is caused by the missing data by which a fraction of small return times are combined to give larger return times. As a consequence, the number of small return times is decreased and the number of intermediate return times is increased. Since the number of missing

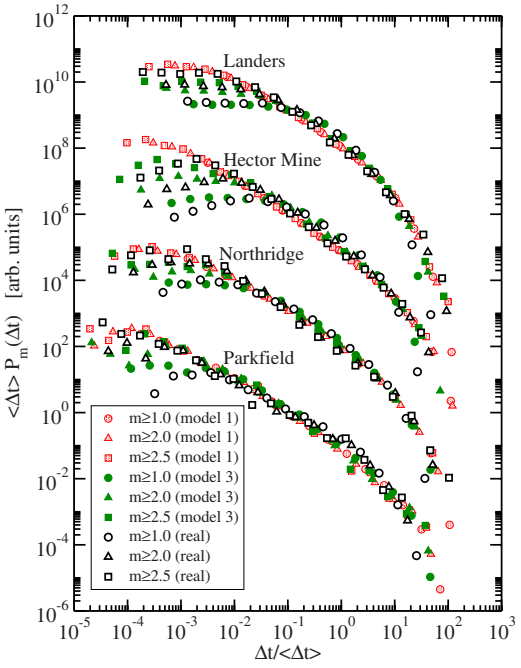

FIG. 7. (Color online) Same as Fig. 6, but with rescaled axes. The x axis has been divided by the mean return time $\langle \Delta t \rangle$ for each data set, and the y axis has been multiplied by $\langle \Delta t \rangle$, respectively. In addition to Fig. 6, the data of model 1 (dotted symbols) are also shown.

data points depends on the threshold, this leads to the observed deviations from scaling, which become more pronounced with an increasing mainshock magnitude.

The agreement between model 3 and the observational data is substantial for small return times, where only small deviations occur for Hector Mine, and even quantitative for intermediate and large return times. We consider it as remarkable that this agreement has been reached without any additional fitting parameters, since γ_1, γ_2, and m_2 have been fixed previously.

IV. CONCLUSION

In this paper we extended the epidemic-type and fully self-similar BASS model to account for the role of missing data at low magnitudes and short times after the mainshock, and applied our model to the aftershock sequences of four Californian earthquakes. The model contains three parameters, one for the threshold, above which the catalogs are complete, and two parameters specifying the fraction of observed data below the threshold. We found that the observed anomalies in the frequency-magnitude scaling could be described quantitatively by this model. We also showed that for the same set of parameters the model was able to reproduce the anomalies in the temporal decay of aftershocks, as well as the behavior of the PDF of the return times. In addition, we showed that for large mainshocks with magnitude M the fraction of observed data with small magnitudes roughly decreases as $10^{-(M-5.3)^2}$. As a consequence, the catalogs of documented earthquakes are considerably more incomplete in aftershock sequences of big events than of small ones.

We would like to emphasize that our model does not include any kind of correlation among the events of an aftershock sequence. The data have been constructed in an uncorrelated way, and also the missing data have been eliminated randomly in a probabilistic manner. We cannot exclude the possibility that, in addition to the trendlike behavior of the magnitudes introduced by the missing data, there may also exist correlations between the observed events. Here we have shown that we can explain all kinds of anomalies by the assumption of uncorrelated data alone. We can exclude the case that the anomalies are exclusively due to long-term correlations, since the scaled PDFs of the return times of long-term correlated data collapse for different thresholds [40], which is absent in the aftershock sequences of large mainshocks.

[1] M. Båth, Tectonophysics **2**, 483 (1965).
[2] B. Gutenberg and C. F. Richter, Bull. Seismol. Soc. Am. **34**, 185 (1944).
[3] F. Omori, J. Coll. Sci., Imp. Univ. Tokyo **7**, 111 (1894).
[4] A. Helmstetter, Y. Y. Kagan, and D. D. Jackson, Bull. Seismol. Soc. Am. **96**, 90 (2006).
[5] Y. Y. Kagan, Bull. Seismol. Soc. Am. **94**, 1207 (2004).
[6] B. Enescu, J. Mori, and M. Miyazawa, J. Geophys. Res. **112**, Bj04310 (2007).
[7] B. Lolli and P. Gasperini, Tectonophysics **423**, 43 (2006).
[8] Z. Peng, J. E. Vidale, and H. Houston, Geophys. Res. Lett. **33**, L17307 (2006).
[9] Z. Peng, J. E. Vidale, M. Ishiii, and A. Helmstetter, J. Geophys. Res. **112**, B03306 (2007).
[10] The catalogs are provided by the Northern California Earthquake Data Center (NCSN catalog, http://www.ncedc.org/ncedc/catalog-search.html) and by the Southern California Earthquake Center (SCEC catalog, http://www.data.scec.org/catalog_search/date_mag_loc.php). For the Landers, Hector Mine, and Northridge earthquakes the areas are $1.1° \times 1.1°$, $1.0° \times 1.0°$, and $0.6° \times 0.6°$, respectively. The area of the Parkfield earthquakes is an elliptical region centered at 35.9° N and −120.5° W with radii of sizes 0.4° and 0.15° and oriented 137° NW. The data up to 365 days after each mainshock were considered. The data are the same as in Refs. [23,24].
[11] D. L. Turcotte, J. R. Holliday, and J. B. Rundle, Geophys. Res. Lett. **34**, L12303 (2007).
[12] J. R. Holliday, D. L. Turcotte, and J. B. Rundle, Physica A **387**, 933 (2008).
[13] K. R. Felzer, T. W. Becker, R. E. Abercrombie, G. Ekström, and J. R. Rice, J. Geophys. Res. **107**, 2190 (2002).
[14] M. I. Bogachev, J. F. Eichner, and A. Bunde, Phys. Rev. Lett. **99**, 240601 (2007).
[15] S. N. Majumdar, Curr. Sci. **77**, 370 (1999).
[16] A. Helmstetter and D. Sornette, J. Geophys. Res. **107**, 2237

(2002).
[17] A. Helmstetter and D. Sornette, Phys. Rev. E **66**, 061104 (2002).
[18] Y. Ogata, J. Am. Stat. Assoc. **83**, 9 (1988).
[19] J. R. Holliday, D. L. Turcotte, and J. B. Rundle, Pure Appl. Geophys. **165**, 1003 (2008).
[20] R. Shcherbakov and D. L. Turcotte, Bull. Seismol. Soc. Am. **94**, 1968 (2004).
[21] A. Helmstetter, Y. Y. Kagan, and D. D. Jackson, J. Geophys. Res. **110**, B05S08 (2005).
[22] T. Utsu, Geophys. Mag. **30**, 521 (1961).
[23] R. Shcherbakov, D. L. Turcotte, and J. B. Rundle, Geophys. Res. Lett. **31**, L11613 (2004).
[24] R. Shcherbakov, D. L. Turcotte, and J. B. Rundle, Bull. Seismol. Soc. Am. **96**, 376 (2006).
[25] S. Lennartz, V. N. Livina, A. Bunde, and S. Havlin, Europhys. Lett. **81**, 69001 (2008).
[26] E. Lippiello, L. de Arcangelis, and C. Godano, Phys. Rev. Lett. **100**, 038501 (2008).
[27] P. Bak, K. Christensen, L. Danon, and T. Scanlon, Phys. Rev. Lett. **88**, 178501 (2002).
[28] A. Corral, Phys. Rev. E **68**, 035102(R) (2003).
[29] A. Corral, Phys. Rev. Lett. **92**, 108501 (2004).
[30] A. Corral, Physica A **340**, 590 (2004).
[31] J. Davidsen and C. Goltz, Geophys. Res. Lett. **31**, L21612 (2004).
[32] A. Corral, Phys. Rev. E **71**, 017101 (2005).
[33] M. Lindman, K. Jonsdottir, R. Roberts, B. Lund, and R. Bodvarsson, Phys. Rev. Lett. **94**, 108501 (2005).
[34] V. Carbone, L. Sorriso-Valvo, P. Harabaglia, and I. Guerra, Europhys. Lett. **71**, 1036 (2005).
[35] R. Shcherbakov, G. Yakovlev, D. L. Turcotte, and J. B. Rundle, Phys. Rev. Lett. **95**, 218501 (2005).
[36] V. N. Livina, S. Havlin, and A. Bunde, Phys. Rev. Lett. **95**, 208501 (2005).
[37] A. Saichev and D. Sornette, Phys. Rev. Lett. **97**, 078501 (2006).
[38] A. Saichev and D. Sornette, Eur. Phys. J. B **49**, 377 (2006).
[39] A. Saichev and D. Sornette, J. Geophys. Res. **112**, B04313 (2007).
[40] A. Bunde, J. F. Eichner, J. W. Kantelhardt, and S. Havlin, Phys. Rev. Lett. **94**, 048701 (2005).